Photochemistry and Photobiology, 2013, 89: 1427–1432

Naphthoxazole-Based Singlet Oxygen Fluorescent Probes†

Rubén Ruiz-González[1], Renzo Zanocco[2], Yasser Gidi[2], Antonio L. Zanocco[2], Santi Nonell*[1] and Else Lemp*[2]

[1]Grup d'Enginyeria Molecular, Institut Químic de Sarrià, Universitat Ramon Llull, Barcelona, Spain
[2]Departamento de Química Orgánica y Fisicoquímica, Facultad de Ciencias Químicas y Farmacéuticas, Universidad de Chile, Santiago, Chile

Received 3 May 2013, accepted 28 May 2013, DOI: 10.1111/php.12106

ABSTRACT

In this study, we report the synthesis and photochemical behavior of a new family of photoactive compounds to assess its potential as singlet oxygen ($^1O_2$) probes. The candidate dyads are composed by a $^1O_2$ trap plus a naphthoxazole moiety linked directly or through an unsaturated bond to the oxazole ring. In the native state, the inherent great fluorescence of the naphthoxazole moiety is quenched; but in the presence of $^1O_2$, generated by the addition and appropriate irradiation of an external photosensitizer, a photooxidation reaction occurs leading to the formation of a new chemical entity whose fluorescence is two orders of magnitude higher than that of the initial compound, at the optimal selected wavelength. The presented dyads outperform the commonly used indirect fluorescent $^1O_2$ probes in terms of fluorescence enhancement maintaining the required specificity for $^1O_2$ detection in solution.

INTRODUCTION

Reactive oxygen species (ROS) are present and participate in many biological processes. Among them, singlet oxygen ($^1O_2$), also well known because its use as a synthetic reagent, plays a key role in the pathological and physiological processes. It can oxidize various kinds of biological molecules (*i.e.* proteins, DNA and lipids), leading to a plethora of deleterious effects that can result in *e.g.* cell death or degenerative diseases (1). Over the years, insight has been gained in the rules that obey its generation, the characters involved and the energy requirements, which has led, among others, to the development of $^1O_2$-based therapies such as photodynamic therapy, in which a drug referred to as the photosensitizer (PS) produces $^1O_2$ upon exposure to light of the appropriate wavelength (2). Despite the major progress made, a better understanding of $^1O_2$ behavior in biological systems is still needed. Of critical importance, techniques and/or methods able not only to detect but also to quantify the concentration of $^1O_2$ both in solution and *in vivo* are still needed (3,4).

Singlet oxygen can be detected through its intrinsic phosphorescence with maximum centered at 1275 nm (5). This is a robust, specific, noninvasive and direct method; but it suffers from weak sensitivity due to the low efficiency for $^1O_2$ emission, particularly in biological media, where the lifetime of $^1O_2$ is very short (3.1 μs) (6) and the phosphorescence quantum yield is very small, *ca* 10^{-7} (7).

Trapping $^1O_2$ with suitable chemical acceptors is also extensively used, as such traps and/or their oxidation products can be monitored more easily through absorption (8,9), fluorescence (3) or ESR (10,11). Fluorogenic probes that develop a bright fluorescence upon reaction with $^1O_2$ have attracted much interest lately as they offer excellent sensitivity and convenience, given the widespread use of fluorescence microscopy techniques. Thus, a two-component system comprising a $^1O_2$ trapping moiety and a suitable fluorophore covalently bound to it is the current paradigm underlying fluorogenic $^1O_2$ probes. In their native state, the luminescence of the emitting moiety is quenched by the trap. Oxidation of the trap by $^1O_2$ eliminates this quenching channel and the luminescence of the fluorophore is recovered.

Several probes have been developed following this principle: DPAX and DMAX (12,13), MTTA-Eu^{3+} (14) and, more recently, SOSG (15–17). All use an anthracene moiety as $^1O_2$ trap that quenches the luminescence of the fluorophore by an electron transfer process. The same concept has been recently used to develop a near-infrared probe, His-Cy, where anthracene has been replaced by a histidine and a cyanine is chosen as fluorophore (18). A common drawback for all the above probes is that the fluorescence increases only moderately after reaction with $^1O_2$, *e.g.* from less than two-fold for His-Cy (18) to *ca* 10-fold for SOSG. Moreover, as electron transfer reactions are strongly dependent on solvent polarity, false-positive signals arise that merely reflect location of the probe in a less polar microenvironment rather than reaction with $^1O_2$, *e.g.* when the probe is in hydrophobic pockets of proteins (16). In addition, the presence of an anthracene moiety in the structure is potentially misleading as anthracene is itself a $^1O_2$ PS that may autooxidize the probe, which further complicates its use (19).

We reasoned that the above problems could be overcome by designing a probe with distinct absorption and fluorescence spectra for the native and oxidized forms. This would allow enhancing the fluorescence of the oxidized form relative to the native probe to an unprecedented level. We report herein the synthesis and characterization of representative members of a new family of $^1O_2$ fluorescence probes based on furan trapping moieties linked to naphthoxazole fluorophores (Fig. 1). Four naphthoxazole derivatives have been synthesized. 2-(2-(Furan-2-yl)ethyl) naphtho[1,2-d]oxazole, **FN-I1**, contains a naphthoxazole linked

*Corresponding author emails: santi.nonell@iqs.url.edu (Santi Nonell); elemp@ciq.uchile.cl (Else Lemp)
†This article is part of the special issue dedicated to the memory of Elsa Abuin.

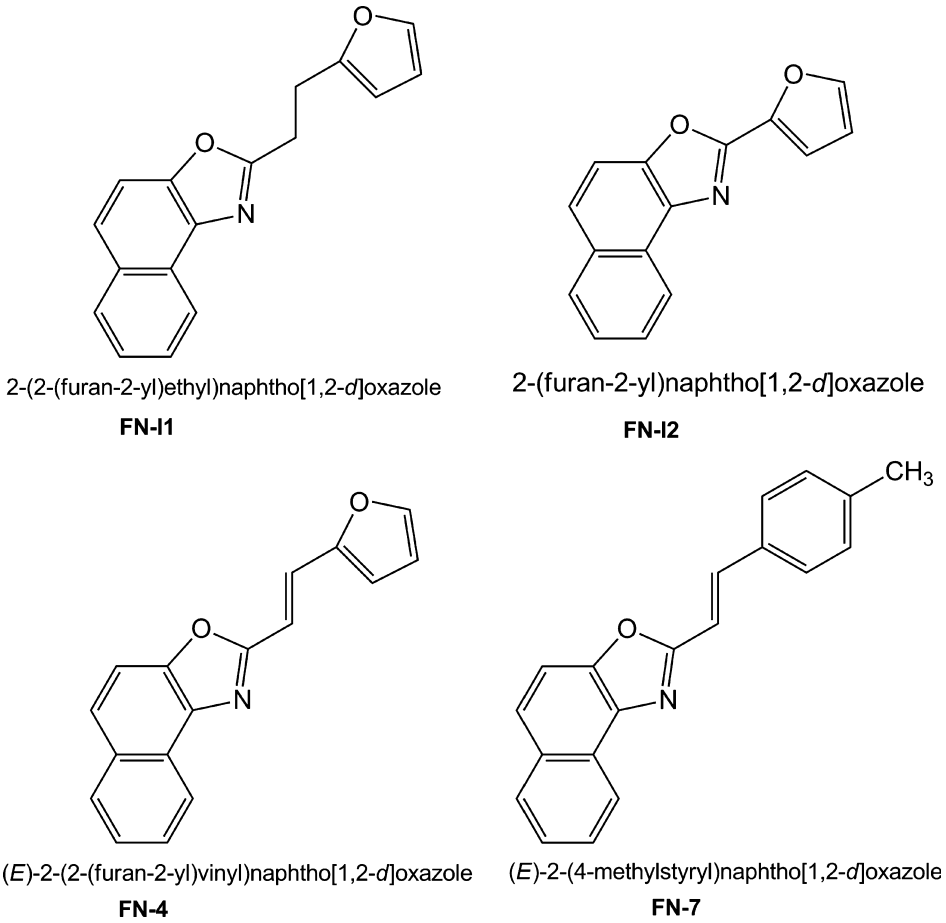

Figure 1. Structure of studied naphthoxazole derivatives.

to a furan through a saturated ethyl bridge. In 2-(furan-2-yl)naphtho[1,2-d]oxazole, **FN-I2**, the furan moiety is bonded directly to the position 2 of the oxazole ring, whereas in (E)-2-(2-(furan-2-yl)vinyl)naphtho[1,2-d]oxazole, **FN-4**, the naphthoxazole and the furan are conjugated through an unsaturated ethylidene link. In the control molecule, (E)-2-(4-methylstyryl)naphtho[1,2-d]oxazole, **FN-7**, the furan ring of **FN-4** has been replaced by a nonreactive tolyl group. Two candidates could be used as $^1O_2$ sensors namely **FN-I2** and **FN-4**, as their fluorescence is boosted by a factor of *ca* 135 and 300, respectively, upon reaction with $^1O_2$.

MATERIALS AND METHODS

Materials. Perinaphthenone, new methylene blue (NMB), anthracene and naphthalene were purchased from Sigma and used as received. All solvents used were UV grade.

(E)-2-(2-(furan-2-yl)vinyl)naphtho[1,2-d]oxazole, FN-4. To a mixture of 2-methylnaphthoxazole (1 mM, 0.15 mL) and furylcarboxaldehyde (0.09 mM, 0.075 mL) in 6 mL of dimethyl sulfoxide, 0.15 mL of aqueous KOH 50% was added. The mixture was stirred by 12 h at room temperature. Addition of 15 mL of water afforded a yellow precipitate which was washed with cold water and cold methanol. Recrystallization from acetonitrile afforded 135 mg of the yellow product, yield 57%, m.p. = 124–126°C. ^{1}H-NMR ($CDCl_3$); δ: 8.51 (d, J = 8.1 Hz, 1H); 7.96 (d, J = 8.1 Hz, 1H); 7.79 (d, J = 9.0 Hz, 1H); 7.69–7.64 (m, 2H); 7.60–7.53 (m, 3H); 7.08 (d, J = 15.9 Hz, 1H); 6.62 (d, J = 3.3 Hz, 1H); 6.51 (m, 1H). MS(ESI) *m/z*: 262.11 [M+H]+, 261.11 [M]+.

2-(2-(furan-2-yl)ethyl)naphtho[1,2-d]oxazole, FN-I1. A quantity of 100 mg (0.38 mmol) of (E)-2-(2-(furan-2-yl)vinyl)naphtho[1,2-d]oxazole, **FN-4**, in 50 mL of dry methanol, was reduced under hydrogen employing 50 mg of Pd-C catalyst. The mixture was stirred during 4 h at room temperature, then, the catalyst was removed by filtration and the solution concentrated *in vacuo.* Recrystallization of the solid residue from petroleum ether 40–60°C, afforded 32 mg of white crystals, 32% yield, m.p. = 120–123°C. ^{1}H-NMR ($CDCl_3$); δ: 8.49 (d, J = 8.0 Hz, 1H); 7.96 (d, J = 8.1 Hz, 1H); 7.76 (d, J = 9.0 Hz, 1H); 7.64 (d, J = 14.2 Hz, 2H); 7.51 (d, J = 14.2 Hz, 1H); 7.33 (s, 1H); 6.27 (d, J = 3.6 Hz, 1H); 6.07 (d, J = 3.6 Hz, 1H); 3.38 (d, J = 7.8 Hz, 2H), 3.30 (d, J = 7.9 Hz, 2H); ppm.

2-(furan-2-yl)naphtho[1,2-d]oxazole, FN-I2. A mixture of 1-amino-2-naphthol (1 mmol), 2-furylcarboxaldehyde (1 mmol) and triethylamine (2 mmol) in 10 mL of dry ethanol was refluxed 3 h under nitrogen. The end of reaction was monitored by thin layer chromatography up to disappearance of the aldehyde. After being cooled to room temperature, the solution was concentrated *in vacuo*, and the crude product recrystallized from acetonitrile to obtain 25% of the product, m.p. 134–136°C. ^{1}H-NMR ($CDCl_3$); δ: 8.54 (d, J = 8.2 Hz, 1H); 8.16 (d, J = 8.2 Hz, 1H); 7.98 (d, J = 8.8 Hz, 1H); 7.81 (d, J = 8.9 Hz, 1H); 7.62–7.54 (m, 3H); 6.66 (d, J = 3.6 Hz, 1H); 6.57 (m, 1H). MS(ESI) m/z: 236.09 [M+H]+, 235.09 [M]+.

(E)-2-(4-methylstyryl)naphtho[1,2-d]oxazole, FN-7. A quantity of 0.15 mL (1 mmol) of 2-methylnaftoxazole, 2 mL of KOH 50% aqueous and 0.11 mL (0.93 mmol) de 4-methyl-benzaldehyde in 6 mL of dimethyl sulfoxide were stirred at room temperature during 12 h to obtain of a greenish yellow. Recrystallization from acetonitrile afforded 145 mg, 56% of the product, m.p. = 127–129°C. ^{1}H-RMN ($CDCl_3$); δ: 8.51 (d, J = 8.1 Hz, 1H); 7.94 (d, J = 8.1 Hz, 1H); 7.77 (d, J = 9.0 Hz, 1H); 7.77 (d, J = 16.2 Hz, 1H); 7.68–7.63 (m, 2H); 7.55–7.49 (m, 3H); 7.22 (d, J = 7.8 Hz, 2H), 7.13 (d, J = 16.2 Hz, 1H); δ 2.38 (s, 3H) ppm.^{13}C-RMN ($CDCl_3$) δ = 162.36, 147.63, 139.86, 138.29, 137.63, 132.61, 131.14, 129.68, 128.58, 127.39, 126.98, 126.29, 126.03, 125.32, 122.07, 113.02, 110.58, 21.44 ppm.

Spectroscopic measurements. Absorption spectra were recorded on a Cary 6000i spectrophotometer (Varian, Palo Alto, CA). Fluorescence emission spectra were recorded on a Spex Fluoromax-4 spectrofluorometer (Horiba Jobin-Ybon, Edison, NJ) or on a PC1 spectrofluorimeter (ISS, Champaign-Urbana). Fluorescence quantum yields (Φ_F) were measured by the comparative method described by Eaton and Demas (20,21), using quinine sulfate in 0.1 N sulfuric acid ($\Phi_F = 0.55$) or naphthalene in ethanol ($\Phi_F = 0.21$) as references (22). The absorbance of sample and reference solutions was set below 0.1 at the excitation wavelength and the fluorescence spectra were corrected using rhodamine G as reference. Sample quantum yields were evaluated using the following Eq. (1):

$$\Phi_x = \left(\frac{\text{Grad}_x}{\text{Grad}_{\text{Act}}}\right)\left(\frac{\eta_x^2}{\eta_{\text{Act}}^2}\right)\Phi_{\text{Act}} \quad (1)$$

where Grad_X and Grad_{Act} are the slope of integrated fluorescence *vs* absorbance plots for the sample and the actinometer and η_x and η_{Act} are the refractive index of sample and actinometer solutions respectively. All measurements were carried out in nitrogen-purged solutions at (20.0 ± 0.5)°C. Fluorescence decays were recorded with a time-correlated single photon counting system (Fluotime 200; PicoQuant GmbH, Berlin, Germany) equipped with a red-sensitive photomultiplier. Excitation was achieved by means of a 375 nm picosecond diode laser working at 10 MHz repetition rate. The counting frequency was maintained always below 1%. Fluorescence lifetimes were analyzed using PicoQuant FluoFit 4.0 software. Light irradiations were performed by means of a SORISA Photocare LED light source applying a power of 25 mW cm^{-2} for every tested wavelength.

Singlet oxygen measurements. The phosphorescence of $^1O_2$ was detected by means of a customized PicoQuant Fluotime 200 system described in detail elsewhere (23). A diode-pumped pulsed Nd:YAG laser (FTSS355-Q; Crystal Laser, Berlin, Germany) working at 10 kHz repetition rate was used for excitation. A 1064 nm rugate notch filter (Edmund Optics, UK) was placed at the exit port of the laser to remove any residual component of its fundamental emission in the near-IR region. The luminescence exiting from the side of the sample was filtered by two long-pass filters of 355 and 532 nm (Edmund Optics, York, UK) and two narrow bandpass filters at 1275 nm (NB-1270-010, Spectrogon, Sweden; bk-1270-70-B, bk Interferenzoptik, Germany) to remove any scattered laser radiation. A near-IR sensitive photomultiplier tube assembly (H9170-45; Hamamatsu Photonics Hamamatsu City, Japan) was used as the detector at the exit port of the monochromator. Photon counting was achieved with a multichannel scaler (PicoQuant's Nanoharp 250). Time-resolved emission signals S_t were analyzed using the PicoQuant FluoFit 4.0 data analysis software to extract lifetime (τ_T and τ_Δ) and amplitude (a) values. Quantum yields for $^1O_2$ production (Φ_Δ) were calculated from the amplitudes using the following Eqs. (2)–(4):

$$S_t = a \times \frac{\tau_\Delta}{\tau_\Delta - \tau_T} \times \left(e^{-t/\tau_\Delta} - e^{-t/\tau_T}\right) \quad (2)$$

$$a \propto \Phi_\Delta \quad (3)$$

$$\Phi_\Delta(\text{sample}) = \Phi_\Delta(\text{ref}) \times \frac{a_{\text{sample}}}{a_{\text{ref}}} \quad (4)$$

Perinaphthenone was used as reference for which $\Phi_\Delta = 1$ was taken (24).

The rate constant for $^1O_2$ quenching by the dyads (k_q) was determined by measuring the $^1O_2$ lifetime as a function of the dyad concentration. $^1O_2$ was generated by 50 μM NMB and the concentration of the dyads was varied in the range (0.1–1 mM). A plot of the reciprocal lifetime *vs* the concentration of the dyad afforded k_q as the slope of the linear-fit Eq. (5),

$$\frac{1}{\tau_\Delta} = \frac{1}{\tau_\Delta^0} + k_q[\text{Dyad}] \quad (5)$$

where τ_Δ^o is the $^1O_2$ lifetime in the neat solvent.

RESULTS

Photophysical characterization

FN-4 is a dyad composed by a furan ring linked to a naphthoxazole moiety through an ethylidene group. The absorption spectrum is dominated by a main band with maximum at 367 nm and a second weaker band at 314 nm (Fig. 2a) that compares reasonably well with the values of 387 and 314 nm obtained from TD-DFT calculations using G09W. The position of the bands follows no obvious trend with the solvent polarity (Table S1). The high values of molar absorptivity, *ca* 3×10^4 M^{-1} cm^{-1} in all solvents except in water, and the molecular orbital analysis of the minimum energy structure obtained from DFT calculations, indicate a π, π^* transition. A similar behavior of the absorption properties was observed for **FN-I2** (Table S2), in which the furan ring is linked directly to the naphthoxazole moiety, and for **FN-7**, in which a nonreactive tolyl substituent replaces the furan moiety. When the linker is saturated (**FN-I1**) spectral bands shift substantially to the blue (λ_{max} = 322 nm) and become more structured. These results correlate with the distinct degree of electronic coupling between the aromatic moiety and the naphthoxazole fluorophore. Similar trends are observed in the maximum of the fluorescence spectra (Fig. 2b) consistent with the reports for related benzoxazole derivatives (25).

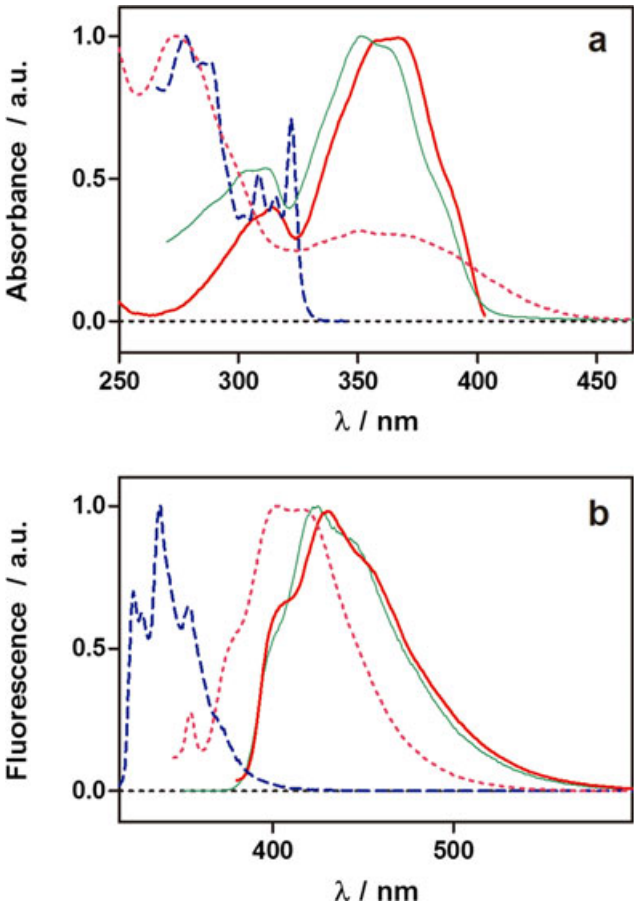

Figure 2. Normalized absorption (a) and fluorescence (b) spectra of **FN-I1** (dashed), **FN-I2** (dotted), **FN-4** (solid) and **FN-7** (light solid) in methanol.

Aryl oxazoles typically exhibit a very high fluorescence quantum yield (Φ_F), in the 0.7–1.0 range (26,27). Among all studied compounds, this is observed only for **FN-I1** ([Φ_F = 0.93] in methanol). In contrast, **FN-4** and **FN-7** show high Φ_F values in low-polarity solvents only, the quantum yield decreasing by 1–2 orders of magnitude as the solvent polarity increases (Tables S1 and S3). However, for (E)-4-(2-(naphtho[1,2-d]oxazol-2-yl)vinyl) benzonitrile, an **FN-7** analogue in which the methyl group is replaced by the strong electron-attractor cyano group, the fluorescence quantum yields are close to one in all solvents, irrespective of their polarity (A. L. Zanocco, unpublished). Finally, **FN-I2** is scantly fluorescent even in nonpolar solvents (Table S2). These results indicate that electron-rich aromatic moieties can act as effective quenchers of naphthoxazole fluorescence in conjugated dyads and, particularly, in polar protic environments, likely due to a charge–transfer interaction. Thus, furyl-oxazole dyads fulfill the first condition requested for a potential $^1O_2$ probe namely that the fluorescence is severely quenched in their native form, thus deserving further scrutiny.

Reactivity toward singlet oxygen

The ability of the dyads to react with $^1O_2$ has been studied by monitoring changes in their absorption and fluorescence properties. No changes could be recorded for **FN-I1** and **FN7**, as expected. In the case of **FN-4**, reaction with $^1O_2$ in methanol caused bleaching of the main band at 367 nm and the growth of a new band in the 325–350 nm region (Fig. 3a). The clear isosbestic point at 348 nm suggests a clean transformation to a single photoproduct (hereafter **FN-4OX**). This was confirmed by HPLC experiments that, after 95% **FN-4** (t_r = 14.3 min) consumption, show the formation of a main product at t_r = 8.3 min and several minor secondary products (Figure S1). Experiments to identify reaction products are in progress; however, furan is well known to selectively react with $^1O_2$ through an endoperoxidation reaction, whereby the primary endoperoxide evolves to different end products depending on the structure of the furan derivative and the solvent (28–30). Involvement of $^1O_2$ in the process was unequivocally demonstrated by the inhibitory effect of selective $^1O_2$ quenchers (Figure S2). Most effective were α-terpinene and sodium azide that inhibited the **FN-4** photooxidation by *ca* 90%. DABCO was able to diminish the **FN-4** consumption to a lesser extent. A strong fluorescence increase and a concomitant shift of the fluorescence peak to the blue could also be observed (Fig. 3c), the excitation spectra of the original and final fluorescence bands being markedly different, implying that they correspond to different chemical species (Fig. 3a, inset). The spectral overlap is minimized at 330 nm, which suggests that this excitation wavelength should be chosen to maximize the fluorescence of **FN-4OX**. As shown in Fig. 4, the fluorescence intensity at 378 nm is enhanced by more than 300-fold. Compared with SOSG, the fluorescence enhancement of **FN-4** is 30-fold larger.

In a similar fashion to that observed for **FN-4**, emission of **FN-I2** also increases considerably upon reaction with $^1O_2$ in methanol (Fig. 3d), concomitant with the bleaching of the low-energy absorption band at 367 nm (Fig. 3b). Both the absorption and fluorescence spectra reveal the appearance of new bands shifted to the blue. The absorption spectra show a clear isosbestic point at 352 nm, suggesting the formation of a single photoproduct as for **FN-4**. Excitation at 333 nm maximizes the system emission, which increases by a factor *ca* 135 at 363 nm (Fig. 4).

The results above demonstrate that the new family of naphthoxazole dyads represented by compounds **FN-4** and **FN-I2** outperform any other fluorescent probe currently available for monitoring $^1O_2$. The key novelty of the system relies on the fact that the fluorophore in the photooxidation adduct is different from that in the initial species. Thus, spectral changes arise that elicit the selection of optimal excitation wavelengths to enhance the fluorescence of the photoproducts.

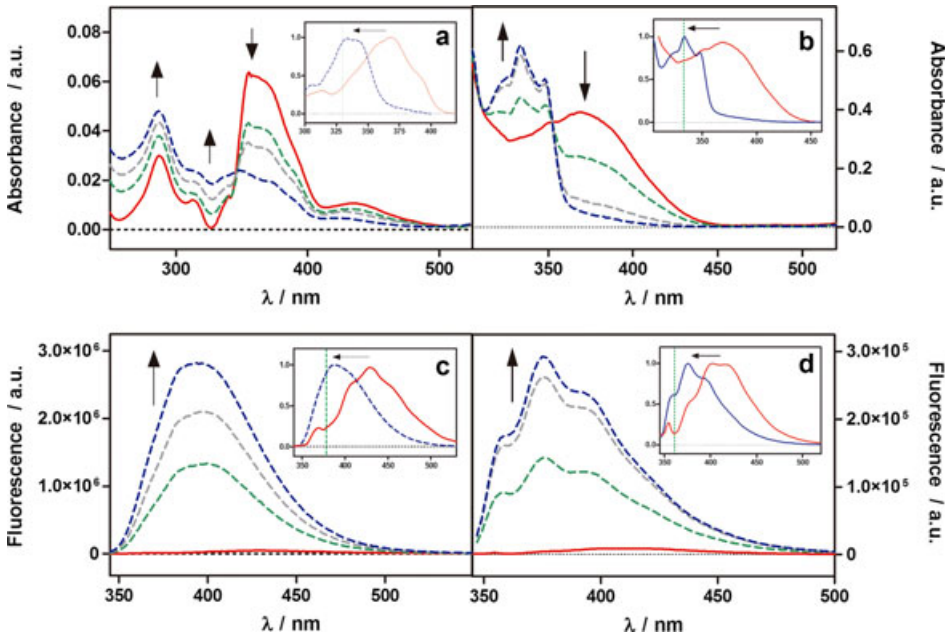

Figure 3. Absorption (a,b) and fluorescence (c,d) spectra of **FN-4** (a,c) and **FN-I2** (b,d) before (solid line) and after (dashed lines) reaction with $^1O_2$. The photosensitizer was new methylene blue 1 μM, the irradiation wavelength was 635 ± 15 nm and the experiments were carried out in aerated methanol. Insets show normalized excitation (a,b) and fluorescence (c,d) spectra to facilitate their comparison.

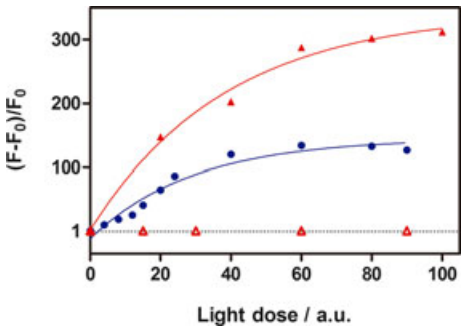

Figure 4. Fluorescence enhancement of **FN-4** (solid triangles; λ_{exc} = 330 nm; λ_{obs} = 378 nm) and **FN-I2** (solid circles; λ_{exc} = 333 nm; λ_{obs} = 363 nm) upon external generation of $^1O_2$ in methanol. Open triangles stand for **FN-4** fluorescence intensity changes upon cumulative irradiation at 355 nm. *F* stands for the fluorescence intensity at each point of study whereas F_0 refers to the background fluorescence.

Table 1. Summary of photophysical, $^1O_2$ production and reactivity data in MeOH for the compounds under study.

Compound	λ_{exc} (nm)	ε (M^{-1} cm^{-1})	Φ_F	k_q (M^{-1} s^{-1})	Φ_Δ*
FN-4	367	30 060	0.014	9.1×10^5	0.003
FN-I1	322	13 940	0.930†	1.9×10^7	0.070
FN-I2	367	31 721	0.032	2.1×10^7	0.009
FN-7	351	32 516	0.050	0.0033‡	0.004

*Perinaphthenone in methanol (Φ_Δ = 1.0) was used as standard; λ_{exc} = 355 nm (24); †Naphthalene in ethanol (Φ_F = 0.21) was used as standard (22). Excitation wavelength was λ_{exc} = 280 nm (for **FN-I1**); ‡Acetonitrile as solvent.

The rate constant for $^1O_2$ quenching by the dyads (k_q) was determined by time-resolved detection of $^1O_2$ phosphorescence at 1275 nm (5,23). Increasing concentrations of the dyads enhanced the decay rate of $^1O_2$ in a linear fashion. The slope of the plots afforded the k_q values, which are collected in Table 1. Interestingly, the value for **FN-4** (vinyl bridge) is 20-fold smaller than that for **FN-I1** (ethyl bridge) and for **FN-I2** (direct link), and about 40-fold smaller than for isolated 2-methylfuran: $k_q = 9.9 \times 10^7$ M^{-1} s^{-1} in methanol (31), which confirms the strong electronic delocalization of the furan ring across the vinyl bridge in **FN-4**. Notice that the fluorescence enhancements do not correlate with k_q. Finally, the low k_q value for **FN-7** confirms that naphthoxazole derivatives lacking the furyl substituent are essentially unreactive toward $^1O_2$.

Self-sensitization of $^1O_2$ by the dyads and reactivity toward other ROS

A drawback of SOSG is the growth of fluorescence due to self-sensitization of $^1O_2$ (19). Other dyads lack selectivity toward $^1O_2$ and react also with different ROS. We investigated whether the naphthoxazole dyads suffered from the same problems. All dyads sensitized the production of $^1O_2$, although with very small quantum yields (Φ_Δ, Table 1 and Figure S3). Nevertheless, Fig. 4 and Figure S4 show that the fluorescence of **FN-4** does not increase upon cumulative irradiation in methanol and that of **FN-I2** actually decreases.

Reactivity toward other ROS was also tested for **FN-I2** and **FN-4.** Negative results for both dyads *vs* both superoxide (KO_2) and H_2O_2 were encountered (Figure S5) indicating a high degree of specificity for $^1O_2$

CONCLUSIONS

FN-4 and **FN-I2** are two examples of successful naphthoxazole-based dyads capable of monitoring $^1O_2$ in solution with unprecedented sensitivity. Photooxidation of the trapping moiety leads to the formation of a new chemical entity whose fluorescence is spectrally different from that of the nonirradiated conjugate. Fluorescence enhancement factors up to 300-fold have been observed taking advantage of the change in spectral properties upon photooxidation. Its added selectivity toward $^1O_2$ and the negligible effects of self-sensitization make naphthoxazole dyads worth of further development as $^1O_2$ fluorescent probes.

Acknowledgements—Financial support for this research was obtained from the Spanish Ministerio de Economóa y Competitividad (CTQ2010-20870-C03-01) and the Chilean Fondo Nacional de Desarrollo Científico y Tecnológico (grants FONDECYT 1120237 and 1080410). R.R.G. thanks the Generalitat de Catalunya (DURSI) and the European Social Fund for a predoctoral fellowship.

SUPPORTING INFORMATION

Additional Supporting Information may be found in the online version of this article:

Figure S1. HPLC chromatograms of **FN-4** before (solid line) and after photooxidation (dashed line) with MB as photosensitizer.

Figure S2. Inhibitory effect of $^1O_2$ selective quenchers for **FN4**.

Figure S3. $^1O_2$ self-sensitization by the dyads in methanol.

Figure S4. FN-4 fluorescence changes upon $^1O_2$ self-sensitization

Figure S5. Selectivity of **FN-4** and **FN-I2** toward other reactive oxygen species.

Table S1. Detailed photophysical characterization of **FN-4** in solution.

Table S2. Detailed photophysical characterization of **FN-I1** in solution.

Table S3. Detailed photophysical characterization of **FN-7** in solution.

REFERENCES

1. Redmond, R. W. and I. E. Kochevar (2006) Spatially resolved cellular responses to singlet oxygen. *Photochem. Photobiol.* **82**, 1178–1186.
2. Agostinis, P., K. Berg, K. A. Cengel, T. H. Foster, A. W. Girotti, S. O. Gollnick, S. M. Hahn, M. R. Hamblin, A. Juzeniene, D. Kessel, M. Korbelik, J. Moan, P. Mroz, D. Nowis, J. Piette, B. C. Wilson and J. Golab (2011) Photodynamic therapy of cancer: An update. *CA Cancer J. Clin.* **61**, 250–281.
3. Soh, N. (2006) Recent advances in fluorescent probes for the detection of reactive oxygen species. *Anal. Bioanal. Chem.* **386**, 532–543.
4. Wu, H., Q. Song, G. Ran, X. Lu and B. Xu (2011) Recent developments in the detection of singlet oxygen with molecular spectroscopic methods. *Trends Anal. Chem.* **30**, 133–141.
5. Nonell, S. and S. E. Braslavsky (2000) Time-resolved singlet oxygen detection. In *Singlet Oxygen, UV-A and Ozone*. (Edited by L. Packer

and H. Sies), *Methods Enzymol.* **319**, 37–49. Academic Press, San Diego.
6. Ogilby, P. R. (2010) Singlet oxygen: There is indeed something new under the sun. *Chem. Soc. Rev.* **39**, 3181–3209.
7. Schweitzer, C. and R. Schmidt (2003) Physical mechanisms of generation and deactivation of singlet oxygen. *Chem. Rev.* **103**, 1685–1758.
8. Gandin, E., Y. Lion and A. Van de Vorst (1983) Quantum yield of singlet oxygen production by xanthene derivatives. *Photochem. Photobiol.* **37**, 271–278.
9. Rabello, B. R., A. P. Gerola, D. S. Pellosi, A. L. Tessaro, J. L. Aparőcio, W. Caetano and N. Hioka (2012) Singlet oxygen dosimetry using uric acid as a chemical probe: Systematic evaluation. *J. Photochem. Photobiol. A* **238**, 53–62.
10. Kalai, T., E. Hideg, I. Vass and K. Hideg (1998) Double (fluorescent and spin) sensors for detection of reactive oxygen species in the thylakoid membrane. *Free Radic. Biol. Med.* **24**, 649–652.
11. Hideg, E. (2004) Detection of free radicals and reactive oxygen species. *Methods Mol. Biol.* **274**, 249–260.
12. Umezawa, N., K. Tanaka, Y. Urano, K. Kikuchi, T. Higuchi and T. Nagano (1999) Novel fluorescent probes for singlet oxygen. *Angew. Chem. Int. Ed. Eng.* **38**, 2899–2901.
13. Tanaka, K., T. Miura, N. Umezawa, Y. Urano, K. Kikuchi, T. Higuchi and T. Nagano (2001) Rational design of fluorescein-based fluorescence probes. Mechanism-based design of a maximum fluorescence probe for singlet oxygen. *J. Am. Chem. Soc.* **123**, 2530–2536.
14. Song, B., G. Wang, M. Tan and J. Yuan (2006) A europium(III) complex as an efficient singlet oxygen luminescence probe. *J. Am. Chem. Soc.* **128**, 13442–13450.
15. Invitrogen—Molecular Probes (2005) Singlet Oxygen Sensor Green Reagent. Available at: http://probes.invitrogen.com/media/pis/mp36002.pdf. Accessed on 18 March 2013.
16. Gollmer, A., J. Arnbjerg, F. H. Blaikie, B. W. Pedersen, T. Breitenbach, K. Daasbjerg, M. Glasius and P. R. Ogilby (2011) Singlet Oxygen Sensor Green®: Photochemical behavior in solution and in a mammalian cell. *Photochem. Photobiol.* **87**, 671–679.
17. Lin, H., Y. Shen, D. Chen, L. Lin, B. C. Wilson, B. Li and S. Xie (2013) Feasibility study on quantitative measurements of singlet oxygen generation using singlet oxygen sensor green. *J. Fluoresc.* **23**, 41–47.
18. Xu, K., L. Wang, M. Qiang, L. Wang, P. Li and B. Tang (2011) A selective near-infrared fluorescent probe for singlet oxygen in living cells. *Chem. Commun.* **47**, 7386–7388.
19. Ragàs, X., A. Jiménez-Banzo, D. Sanchez-Garcia, X. Batllori and S. Nonell (2009) Singlet oxygen photosensitisation by the fluorescent probe Singlet Oxygen Sensor Green®. *Chem. Commun.* **20**, 2920–2922.
20. Demas, J. N. and G. A. Crosby (1971) Measurement of photoluminescence quantum yields—Review. *J. Phys. Chem.* **75**, 991–1024.
21. Eaton, D. F. (1988) Reference materials for fluorescence measurement. *Pure Appl. Chem.* **60**, 1107–1114.
22. Montalti, M., A. Credi, L. Prodi and G. M.T (2006) *Handbook of Photochemistry*, 3rd edn. CRC Press, Boca Raton, FL.
23. Jiménez-Banzo, A., X. Ragàs, P. Kapusta and S. Nonell (2008) Time-resolved methods in biophysics. 7. Photon counting vs. analog time-resolved singlet oxygen phosphorescence detection. *Photochem. Photobiol. Sci.* **7**, 1003–1010.
24. Schmidt, R., C. Tanielian, R. Dunsbach and C. Wolff (1994) Phenalenone, a universal reference compound for the determination of quantum yields of singlet oxygen $O_2(^1\Delta_g)$ sensitization. *J. Photochem. Photobiol. A* **79**, 11–17.
25. Mac, M., B. Tokarczyk, T. Uchacz and A. Danel (2007) Charge transfer fluorescence of benzoxazol derivatives investigation of solvent effect on fluorescence of these dyes. *J. Photochem. Photobiol. A* **191**, 32–41.
26. Machado, A. E., J. de Miranda, S. Guilardi, D. Nicodem and D. Severino (2003) Photophysics and spectroscopic properties of 3-benzoxazol-2-yl-chromen-2-one. *Spectrochim. Acta A Mol. Biomol. Spectrosc.* **59**, 345–355.
27. Fayed, T. (2004) Probing of micellar and biological systems using 2-(p-dimethylaminostyryl)benzoxazole—An intramolecular charge transfer fluorescent probe. *Colloids Surf. A* **236**, 171–177.
28. Gollnick, K. and A. Griesbeck (1985) Singlet oxygen photooxygenation of furans—isolation and reactions of (4 2)-cycloaddition products (unsaturated sec-ozonides). *Tetrahedron* **41**, 2057–2068.
29. Lemp, E., A. Zanocco and E. Lissi (2003) Linear free energy relationship analysis of solvent effects on singlet oxygen reactions. *Curr. Org. Chem.* **7**, 799–819.
30. Clennan, E. L. and A. Pace (2005) Advances in singlet oxygen chemistry. *Tetrahedron* **61**, 6665–6691.
31. Wilkinson, F., W. P. Helman and A. B. Ross (1995) Rate constants for the decay and reactions of the lowest electronically excited singlet state of molecular oxygen in solution. An expanded and revised compilation. *J. Phys. Chem. Ref. Data* **24**, 663–677.